2163-32

College on Soil Physics: Soil Physical Properties and Processes under Climate Change

30 August - 10 September, 2010

Sediment transport from interrill areas under wind-driven rain

Gunay Erpul
*University of Ankara
Turkey*

Sediment transport from interrill areas under wind-driven rain

G. Erpul[a,*], L.D. Norton[b], D. Gabriels[c]

[a]*Department of Soil Science, Faculty of Agriculture, Ankara University, Diskapi, Ankara 06110, Turkey*
[b]*USDA-ARS National Soil Erosion Research Laboratory, 1196 SOIL Building, Purdue University, West Lafayette, IN 47907-1196, USA*
[c]*Department of Soil Management and Soil Care, Ghent University, Coupure Links 653, B 9000 Ghent, Belgium*

Abstract

In nature, erosive rainstorms are usually associated with high winds. Therefore, a quantification of wind and rain interactions and the effects of wind on detachment and transport processes provides a great opportunity for a given prediction technology to improve the estimation of erosion. This paper presents experimental data obtained on interrill erosion processes under wind-driven rain. In a wind tunnel facility equipped with a rainfall simulator, windless rains and the rains driven by horizontal wind velocities of 6, 10, and 14 m s^{-1} were applied to three agricultural soils packed into 20 by 55 cm soil pan at both windward and leeward slopes of 7, 15, and 20%. Wind-driven rainsplash transport was measured by trapping the splashed particles at distances on a 7-m uniform slope segment in the upslope and downslope directions, respectively, for windward and leeward slopes. The process was adequately described by relating the rainsplash transport rate to the rainfall parameter, fluxes of rain energy or momentum, and wind shear velocity by log-linear regression technique. Sediment transport by rain-impacted thin flow was measured by collecting sediment and runoff samples at 5-min intervals after runoff onset. This process was also adequately described by rainfall and flow parameters. Comparing the process contribution to the total sediment transport, it is concluded that rainsplash transport is a significant process that should not be neglected in accurately predicting interrill water erosion under wind-driven rain. Mean values for the ratio of rainsplash erosion to the corresponding total sediment transport were 14.6 ± 6.4, 23.9 ± 7.8, and 38.1 ± 8.7% for the rains driven by 6, 10, and 14 m s^{-1} wind, respectively.
© 2003 Elsevier Science B.V. All rights reserved.

Keywords: Wind-driven rain; Slope gradient and aspect; Interrill erosion; Rainsplash transport; Thin flow transport

1. Introduction

[Van Heerden (1967)](#) first attempted to determine the rainsplash transport under different combined levels of the variables: wind, angle of incidence, and particle size. He expressed the rainsplash transport in a mathematical form of:

$$Q_s = \sum_{i=1}^{n} m_i x_i \tag{1}$$

where Q_s is the rainsplash transport, and m_i is the mass of a particle, which is splashed over a distance x_i measured along the x-axis. [Savat and Poesen (1981)](#) conducted a series of laboratory experiments to measure the ejected sediment quantities and the mean projected distances by rainsplash. Exponential

curves were fitted for the distribution of splashed sediment as a function of travel distance:

$$m_i = a\,e^{-bx_i} \tag{2}$$

where a and b are the coefficients which depend on the physical properties of the sediment. Assuming a linear relation between kinetic energy and soil detachment, the following formula for the net downslope rain-splash erosion was recommended by Poesen and Savat (1981):

$$Q_s = \frac{KE}{K}[0.31 \sin \theta + 0.0192(D_{50})^{-0.218} \times (1 - e^{-2.42 \sin \theta})] \tag{3}$$

where Q_s is the net downslope rainsplash erosion unit discharge (kg m^{-1} yr^{-1}), KE is the kinetic energy per surface per unit time (J m^{-2} yr^{-1}), K is the resistance to detachment (J kg^{-1}), D_{50} is the median grain size (m), and θ is the slope gradient (°). Eq. (3) essentially explains the relationship between mean travel distance and slope gradient for the rainsplash transport process and the relationship between kinetic energy and soil detachment for the rainsplash detachment process.

In the study of measuring the rainsplash transport under oblique rain, Moeyersons (1983) defined total net saltation flux in the form of Eq. (1), making an assumption that the flux occurs at the same direction as the horizontal velocity component of raindrops, parallel to a surface. The experiment showed that the process depended not only on the slope gradient but also on the slope orientation. Following this observation, Poesen (1985) recommended an improved rainsplash transport model for the oblique rain on bare slopes. In order to include the effect of slope aspect, the slope gradient term (θ) in Eq. (3) was replaced by the angle of rain incidence ($\alpha \pm \theta$). In addition, the cosine of the angle of rain incidence [cos($\alpha \pm \theta$)] was inserted into the model to account for variations in kinetic energy dissipation with slope gradient and aspect. Clearly, it is considered here that the detachment rate varies with the slope gradient and aspect under oblique rain, and that the slope effect on the rainsplash transport is greater when rainfall is directed downslope than that when directed upslope.

Wright (1986) stressed the effect of oblique rain in altering the values of the parallel and normal components of the incident raindrop momentum and hence altering the direction and magnitude of the splash asymmetry. Similar to the conclusion of Poesen (1985), this effect was explained by the slope: more momentum is transferred in the down-slope direction and thus the difference in rainsplash transport between upslope and downslope transport increases. However, under wind-driven rain once lifted-up by the raindrop impact, soil particles entrained into splash droplets travel some distance, which varies directly with the wind shear velocity. In such a situation, the wind transports detached particles parallel to the surface irrespective of slope gradient and aspect. This combined rainsplash process of rain and wind has long been well known (Rutin, 1983; Jungerius and Dekker, 1990; De Lima et al., 1992; Van Dijk et al., 1996; Goossens et al., 2000). Jungerius et al. (1981) found that the strong winds together with rain had no difficulty in moving sand in contrast to their expectation that wet sand was not as easily moveable as dry sand. The raindrop impacts induced the process that wind would otherwise be unable of transporting wet and cohesive soil particles. Evidently, considering the effect of wind on physical raindrop impact (Umback and Lembke, 1966; De Lima, 1989, 1990; Pedersen and Hasholt, 1995) and particle transport, rainsplash detachment and transport under wind-driven rain differs from those under windless rain.

The wind-driven rainsplash could also be a significant process to the extent that it might not be a negligible process in accurately predicting interrill soil erosion. In this case, when raindrops first impact bare soil, wind-driven rainsplash process operates alone, and by the time that runoff occurs, produces net transport and provides the first stage of the transport sequence of interrill soil erosion. This reasoning implies that sediment transport by rain-impacted thin flow shows a complementary relationship to the rainsplash, which rapidly becomes less effective as flow depth increases from zero (Moss, 1988).

The essential processes of sediment transport by rain-impacted thin flow are rainsplash detachment and flow-driven transport. In other words, thin flow-driven sediment transport from interrill areas is determined by the interaction of rain and flow parameters as shown by Parsons et al. (1998). Julien and Simon (1985) investigated the applicability of several

sediment transport equations under different hydraulic conditions. The transport capacity of rain-impacted thin flow was characterized by rainfall intensity (I), unit discharge (q), and channel bottom slope (S) by:

$$q_s = KI^a q^b S^c \qquad (4)$$

where q_s is the sediment transport rate by rain-impacted thin flow, and K, a, b, and c are the experimental coefficients. Guy et al. (1987) carried out a laboratory study to investigate the transport capacity of interrill flow. The transport capacity of raindrop-disturbed flows was greatly enhanced by raindrop impact, and 85% of the enhancement was attributed to the raindrop impact and only 15% to the runoff. The simplified model equations based on $I–q–S$ were initially developed, and fluxes of rain energy and momentum provided slightly better results than intensity; however, the differences were small due to the narrow range of raindrop velocities produced by the rainfall simulator.

Kinnell (1993) explored the interrill erosion data of the WEPP (Water Erosion Prediction Project, Nearing et al., 1989), and the process was presented by a quantification of interactions between intensity, discharge and slope:

$$q_s = KQIS_f \qquad (5)$$

where K is the estimate of interrill erodibility, Q is the discharge, and S_f is the friction slope. Zhang et al. (1998) proposed the model equation for interrill sediment delivery in the form developed by Julien and Simon (1985) and Guy et al. (1987):

$$D_i = K_i I q^{1/2} S^{2/3} \qquad (6)$$

where D_i is the interrill sediment delivery per unit area per unit time, and K_i is a relative erodibility parameter. The linear intensity term represented detachment of soil by raindrop impacts and enhancement of transport capacity by a thin flow. The product of $q^{1/2}S^{2/3}$ was considered to represent the sediment transport by flow. The authors also cited that rainfall energy (KE) might replace rainfall intensity (I) because the use of kinetic energy minimizes the potential errors in extrapolating experimental results to rains with different characteristics.

Our study involves evaluating both wind-driven rainsplash and sediment transport by rain-impacted thin flow transport with the objective of improving the understanding of interrill erosion processes under wind-driven rain, which commonly occurs in intense erosive storms.

2. Materials and methods

The study was conducted in a wind tunnel rainfall simulator facility at Ghent University, Belgium (Gabriels et al., 1997). A continuous spraying system of downward oriented nozzles was used at the nozzle pressure of 1.5 bar. The nozzles at this operating pressure delivered a median drop size of 1.00, 1.63, 1.53, and 1.54 mm for the windless rains and the rains driven by the wind velocities of 6, 10, and 14 m s^{-1}, respectively. A detailed description of the raindrop size distribution for the simulated rainfalls of the wind tunnel is given by Erpul et al. (1998, 2000). Three loess derived agricultural soils, Kemmel1 sandy loam (57.6% sand, 31.1% silt, and 11.3% clay) and Kemmel2 loam (37.8% sand, 44.5% silt, and 17.7% clay) from the Kemmelbeek watershed (Heuvelland, West Flanders, Belgium) and Nukerke silt loam (32.1% sand, 52.3% silt, and 15.6% clay) from the Maarkebeek watershed (Flemish Ardennes, East Flanders, Belgium) were used in this study. The soil samples were collected from the A_p horizon and air-dried prior to the experiment. Soil was sieved into three aggregate fractions: 1.00–2.75, 2.75–4.80, and 4.80–8.00 mm, and the weighing factors assigned to each fraction were 28, 32, and 40%, respectively, to reconstitute the packing soil. A 5 kg soil sample was then packed loosely into a 55 cm-long and 20 cm-wide pan after the three fractions of aggregates were evenly mixed.

Windless rains and the rains driven by horizontal wind velocities of 6, 10, and 14 m s^{-1} were applied to the soil pan placed at both windward and leeward slopes of 7, 15, and 20%. For each soil and slope aspect, there were three replicates, or 36 runs for a total of 216 rainfall simulations.

Wind velocity profiles were measured up to 2 m-nozzle height with a vane type anemometer and associated recording equipment, and the wind velocity profiles above the soil pan were characterized by

the following logarithmic equation:

$$u(z) = \left(\frac{u_*}{\kappa}\right)\ln\left(\frac{z}{z_0}\right) \text{ for } z > z_0 \qquad (7)$$

where $u(z)$ is the wind velocity at height z, z_0 is the roughness height, u_* is the wind shear velocity, and κ is von Karman's constant. The boundary layer was set at 0.30 m above the soil pan. Subsequently, the reference shear velocities were derived from the logarithmic wind profiles, assuming a fixed roughness height of 0.0001 m for a bare and smoothed soil surface from the relation:

$$z = a\,e^{bu} \qquad (8)$$

where $a = z_0$ and $b = \kappa/u_*$. Average wind velocity profiles regardless of slope gradient and aspect are $0.0001\,e^{1.1148u}$, $0.0001\,e^{0.7480u}$, and $0.0001\,e^{0.5142u}$, and the corresponding reference shear velocities are 0.35, 0.53, and 0.77 m s^{-1} for the reference wind velocities of 6, 10, and 14 m s^{-1}, respectively.

The energy of simulated rainfalls was measured by a piezoelectric ceramic kinetic energy sensor (Sensit™, 2000). The kinetic energy sensor is a 5 cm ceramic disk and works on the piezoelectric effect of a ceramic disc, which produces electric charges proportional to the kinetic energy of impacting raindrops. The Sensit essentially has two outputs: kinetic energy units and number of raindrop impacts. The voltage output of the Sensit was calibrated for kinetic energy with vertically falling water drops of known size and known fall velocity. Drop size ranged between 2.15 and 4.96 mm, and their terminal vertical fall velocities were derived from the nomograph of Laws (1941). The functional relationship obtained by the kinetic energy sensor between the kinetic energy and the horizontal wind velocity was in the form of:

$$KE = 6E - 06\,e^{0.2184u} \qquad (9)$$

where E notation shows 'times 10 to the power', KE in Joules, and u in m s^{-1}. The calculated resultant impact velocities (V_R) of median drop sizes for the windless rains and the rains driven by the reference wind velocities of 6, 10, and 14 m s^{-1} were 4.38 ± 0.58, 4.64 ± 0.56, 7.64 ± 0.60, and 10.48 ± 0.57 m s^{-1}, respectively. The sensor measurement showed that an exponential relationship existed between the energy of the simulated rains and the horizontal wind velocity. The increase in rain energy was mainly ascribed to the increase in the resultant raindrop impact velocity since the raindrop size distribution did not change significantly in the rains driven by 6, 10 and 14 m s^{-1} in the wind tunnel facility (Erpul et al., 1998, 2000).

The intensity of simulated rains was directly measured with 5 small collectors on the inclined plane with respect to the prevailing wind direction. That is, the collectors were placed next to the soil pan with the same slope gradient and aspect as the soil pan during each run. In this way, the intensity measurements were made truly representative for each run without any need for correction due to the rain inclination gained from horizontal wind velocity and slope gradient and aspect (Sharon, 1980; De Lima, 1990). From the direct intensity measurements, the average angle of rain incidence between the wind vector and the plane of the surface ($\alpha \mp \theta$) was calculated using the cosine law of spherical trigonometry (Sellers, 1965):

$$\phi = \frac{I_a}{I} = \cos(\alpha \mp \theta) \qquad (10)$$

where ϕ is the impact efficiency of wind-driven raindrops, I_a is the actual intensity (mm h^{-1}), I is the rainfall intensity in respect to a plane normal to the rain vector (mm h^{-1}), α is the raindrop inclination from vertical (°), and θ is the slope gradient (°). In fact, Eq. (10) indicates that the actual rate of wind-driven raindrop impacts per unit area varies with the rain inclination and slope gradient and aspect. The calculated rain inclination was 53.0 ± 11.5, 68.2 ± 7.6, and $73.5 \pm 6.6°$ for the rains driven by wind velocities of 6, 10, and 14 m s^{-1}, respectively. The angles refer to the average values generalized over the raindrop size range.

In the present study, we assumed rainsplash detachment rate under inclined rain is related to the normal component of raindrop impact velocity (Heymann, 1967; Springer, 1976; Gilley et al., 1985; Gilley and Finkner, 1985). Accordingly, the fluxes of rain energy (KE) or momentum (M) based on the normal velocity of raindrop impact were used as a rainfall parameter (Θ):

$$KE = \Xi_a\left(\frac{1}{2}mV_R^2\right)\phi^2 \qquad (11)$$

Table 1
Fluxes of energy (KE) and momentum (M) for the windless rains and the rains driven by the reference wind velocities of 6, 10, and 14 m s^{-1}

u (m s^{-1})	V_R (m s^{-1})	D_{50} (mm)	α (°)	θ (°)	I_a (mm h^{-1})	$\alpha \pm \theta$ (°)	ϕ	KE (W m^{-2})	M (N m^{-2})
0-ww	4.38 ± 0.58[a]	1.00	–	4.0	142	4.0	0.9976	0.377	0.172
		$0.97 \leq D_{50} \leq 1.04$[b]		8.5	140	8.5	0.9890	0.365	0.168
				11.3	134	11.3	0.9806	0.343	0.160
6-ww	4.64 ± 0.56	1.63	53.0 ± 11.5[a]	4.0	90	49.0	0.6561	0.116	0.076
		$1.38 \leq D_{50} \leq 1.84$		8.5	100	44.5	0.7133	0.152	0.092
				11.3	106	41.7	0.7466	0.177	0.102
10-ww	7.64 ± 0.60	1.53	68.2 ± 7.6	4.0	120	64.2	0.4352	0.184	0.111
		$1.50 \leq D_{50} \leq 1.57$		8.5	130	59.7	0.5045	0.268	0.139
				11.3	131	56.9	0.5461	0.317	0.152
14-ww	10.48 ± 0.57	1.54	73.5 ± 6.6	4.0	90	69.5	0.3502	0.168	0.092
		$1.51 \leq D_{50} \leq 1.57$		8.5	103	65.0	0.4226	0.281	0.127
				11.3	112	62.2	0.4664	0.372	0.152
0-lw	4.38 ± 0.58	1.00	–	4.0	165	4.0	0.9976	0.438	0.200
		$0.97 \leq D_{50} \leq 1.04$		8.5	172	8.5	0.9890	0.448	0.207
				11.3	179	11.3	0.9806	0.459	0.214
6-lw	4.64 ± 0.56	1.63	53.0 ± 11.5	4.0	126	57.0	0.5446	0.112	0.088
		$1.38 \leq D_{50} \leq 1.84$		8.5	112	61.5	0.4772	0.076	0.069
				11.3	94	64.3	0.4337	0.053	0.053
10-lw	7.64 ± 0.60	1.53	68.2 ± 7.6	4.0	92	72.2	0.3057	0.070	0.060
		$1.50 \leq D_{50} \leq 1.57$		8.5	61	76.4	0.2351	0.027	0.030
				11.3	51	79.5	0.1822	0.014	0.020
14-lw	10.48 ± 0.57	1.54	73.5 ± 6.6	4.0	66	77.5	0.2164	0.047	0.042
		$1.51 \leq D_{50} \leq 1.57$		8.5	42	82.0	0.1392	0.012	0.017
				11.3	34	84.8	0.0906	0.004	0.009

u, horizontal wind velocity (ww: windward; lw: leeward); V_R, resultant raindrop impact velocity; D_{50}, median drop size; α, rain inclination from vertical; θ, slope gradient; I_a, actual rainfall intensity; ($\alpha \pm \theta$), angle of rain incidence; ϕ, cosine of angle of rainfall incidence [$= \cos(\alpha \pm \theta)$].

[a] Standard deviations of the resultant raindrop impact velocity and the rainfall inclination are given next to the mean value with ± sign.
[b] 95% confidence interval on mean values of D_{50}.

$$M = \Xi_a(mV_R)\phi \qquad (12)$$

where KE and M are in W m^{-2} and N m^{-2}, respectively, m is the raindrop mass in kg, and Ξ_a is the number of raindrops in # m^{-2} s^{-1} and calculated by:

$$\Xi_a = \frac{I_a}{\forall} \qquad (13)$$

where I_a is in m s^{-1}, and $\forall$ is the raindrop volume in m^3.

Rainsplash transport was evaluated by the amount of the splashed particles trapped at set distances on a 7 m uniform slope segment. Troughs were placed in both upslope and downslope directions for windless rain, and in upslope and downslope directions, respectively, for windward and leeward slopes for wind-driven rain. For windless rain, splashboards were also positioned to collect side splash. The soil particles trapped in the collecting troughs were washed, oven-dried, and weighed. Mass distribution curves were then determined for windless and wind-driven rains, from which rainsplash transport rates were calculated based on Eq. (1) by:

$$Q_s = \frac{1}{At_r} \int m_i \, dx \qquad (14)$$

where Q_s is in g m^{-1} min^{-1}, A is the collecting trough area (1.20 m $\times$ 0.14 m = 0.168 m^2), and t_r is the time (min) during which rainsplash process occurred. It is important here to note that since vertically falling raindrops produced particle movement in all directions, differences between amounts of upslope and downslope splash and amounts of left and right side splash were regarded as the measures of net particle transport for windless rains (Van Heerden, 1967; Poesen, 1985). On the other hand, the particle movement was unidirectional and in the prevailing wind direction (De Lima, 1989) under wind-driven rains. Therefore, only upslope net particle movements were observed in the wind-driven rains on windward

slopes and downslope movements in the wind-driven rains on leeward slopes. At last, the wind-driven rainsplash process was related to the rainfall parameter and the wind shear velocity and analyzed using a log-linear regression technique (SAS, 1995) by:

$$Q_s = k_1 \Theta^{a_1} u_*^{b_1} \tag{15}$$

where k_1 is the relative soil transport parameter for the wind-driven rainsplash process, u_* is the wind shear velocity (m s^{-1}), and a_1 and b_1 are the regression coefficients.

Simulated rainfalls were conducted under freely drained conditions, and generally steady-state soil loss and runoff rates were attained within 45 min in

Table 2
Summary of the data for the measured rainsplash transport rates (Q_s) for three soils

u (m s^{-1})	S (m m^{-1})	u_* (m s^{-1})	Rainsplash transport rate, Q_s (g m^{-1} min^{-1})						n
			Nukerke		Kemmel1		Kemmel2		
			Mean	Stdev.	Mean	Stdev.	Mean	Stdev.	
0-ww	0.07	–	0.64	0.14	1.02	0.89	0.49	0.02	3
	0.15		0.90	0.28	1.31	0.72	1.47	0.08	3
	0.20		1.59	0.35	1.47	0.31	1.25	0.33	3
6-ww	0.07	0.35	2.25	0.22	2.02	0.11	1.69	0.43	3
	0.15		2.81	0.35	3.11	0.31	2.24	0.33	3
	0.20		4.21	0.48	3.80	0.24	2.74	0.35	3
10-ww	0.07	0.53	11.03	0.48	9.02	1.43	8.91	1.60	3
	0.15		11.03	0.44	10.70	1.41	10.73	1.51	3
	0.20		16.03	1.60	20.83	2.22	12.90	3.23	3
14-ww	0.07	0.77	16.65	1.35	11.70	0.93	10.81	1.66	3
	0.15		29.41	3.13	23.64	3.01	25.76	5.59	3
	0.20		41.60	6.38	35.91	3.59	38.78	6.75	3
0-lw	0.07	–	0.60	0.15	0.54	0.12	0.71	0.30	3
	0.15		0.75	0.12	0.91	0.03	1.09	0.19	3
	0.20		1.19	0.05	1.31	0.26	1.18	0.05	3
6-lw	0.07	0.35	4.49	0.40	1.27	0.10	2.73	0.38	3
	0.15		1.54	0.06	0.86	0.05	2.78	0.44	3
	0.20		1.62	0.14	1.12	0.12	1.57	0.09	3
10-lw	0.07	0.53	4.31	0.30	3.72	0.23	3.21	0.16	3
	0.15		1.50	0.09	1.09	0.14	1.58	0.09	3
	0.20		1.58	0.26	0.96	0.10	1.07	0.04	3
14-lw	0.07	0.77	5.16	0.23	7.32	0.70	5.68	0.43	3
	0.15		2.74	0.26	1.56	0.22	2.00	0.26	3
	0.20		1.10	0.09	0.95	0.11	0.92	0.15	3

Mean values are given in the table, however, statistical analyses are performed with individual data points u horizontal wind velocity (ww: windward; lw: leeward); S, channel bottom slope; u_* wind shear velocity.

windless rains and the wind-driven rains on windward slopes. However, particularly in the rains driven by wind velocities of 10 and 14 m s^{-1} on the leeward slopes of 15 and 20%, time to runoff changed greatly, and overland flow generation was retarded due to the lesser amount of rain interception. In these cases, the rain stopped after 45 min in order to collect wind-driven rainsplash samples, then, an additional 45 min rainfall run was needed to be able to collect sediment and runoff samples. During each rainfall application and after runoff started sediment and runoff samples were collected at 5 min intervals at the bottom edge of the pan using wide-mouth bottles and were determined gravimetrically. Total sediment and runoff values, and the time during which the process occurred were used in calculation of sediment transport by rain-impacted thin flow (q_s). The following model was analyzed for the sediment transport by rain-impacted thin flow based on interrill erosion mechanics:

$$q_s = k_2 \Theta^{a_2} q^{b_2} S^{c_2} \tag{16}$$

where q_s is in g m^{-1} min^{-1} and q is in m^2 min^{-1}, and S in mm^{-1}. k_2 is the relative soil transport parameter for thin flow-driven process, and a_2, b_2, and c_2 are the regression coefficients. Finally, total interrill erosion under wind-driven rain was defined by:

$$q_i = Q_s + q_s \tag{17}$$

where q_i is the total interrill sediment transport.

3. Results and discussion

3.1. Wind-driven rainsplash transport

The rainsplash process acted alone until runoff occurred, and net soil transport was affected by slope and wind, respectively, for windless and wind-driven rains. The observed distance of particle travel was up to 0.40 m under windless rains and ranged from 3 to 7 m depending on the gradient of wind velocity profile under wind-driven rains. For example, the particle trajectories were complete at 3 m in the rains driven by 6 m s^{-1} wind velocity, and at 7 m in the rains driven by 10 and 14 m s^{-1} wind velocities. On the other hand, the rate at which soil particles were entrained into the air was a function of such physical

raindrop parameters as velocity, frequency, and angle of impact. Values for the fluxes of rain energy and momentum and the measured rainsplash rates are presented in Tables 1 and 2, respectively. The statistical fit of the power law models, of which general form is given by Eq. (15), is presented in Table 3, and the equations for the combined data from three soils are:

$$Q_s = 119.95 \text{KE}^{0.81} u_*^{2.09} \tag{18}$$

$$Q_s = 582.24 M^{1.27} u_*^{2.27} \tag{19}$$

Units of the variables are presented in Tables 1 and 2. The models performed equally well and provided similar R^2 values, which were ≥ 0.94 for the three soils (Fig. 1). The analysis of variance also showed that K_1, a_1, and b_1 were significant at $P = 0.0001$ level of significance. Additionally, the coefficient of efficiency, E (Nash and Sutcliffe, 1970) was calculated from the predicted and measured values to quantitatively evaluate the performance of each model. Actually, E is the ratio of the mean square

Table 3
Statistical analyses for the equation of the wind-driven rainsplash transport (Q_s) developed by log-linear regression technique for three soils and for the combined data from three soils

Soil	$Q_s = k_1 \text{KE}^{a_1} u_*^{b_1}$				
	k_1[a]	a_1	b_1	R^2	E[b]
Nukerke	119.75	0.78	2.00	0.96	0.94
Kemmel1	144.43	0.86	2.32	0.95	0.91
Kemmel2	99.54	0.79	1.95	0.94	0.90
All data	119.95	0.81	2.09	0.94	0.92
	$Q_s = k_1 M^{a_1} u_*^{b_1}$				
	k_1	a_1	b_1	R^2	E
Nukerke	537.91	1.21	2.17	0.96	0.94
Kemmel1	755.31	1.34	2.51	0.95	0.93
Kemmel2	484.08	1.25	2.12	0.95	0.90
All data	582.24	1.27	2.27	0.94	0.92

[a] The model parameters, k_1, a_1 and b_1, in all equations were significant at the $P = 0.0001$ level of significance for the three soils and all data.
[b] The coefficient of efficiency (Eq. (20)).
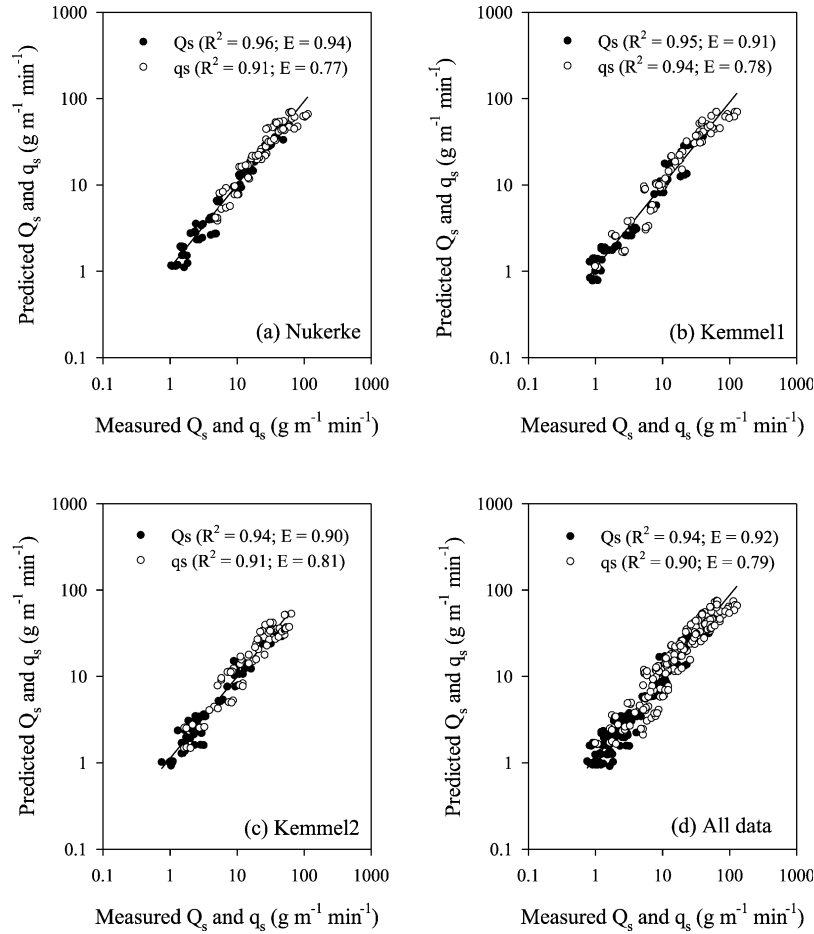
Fig. 1. Measured and predicted transport rates by wind-driven rainsplash (Q_s) and rain-impacted thin flow (q_s) for Nukerke silt loam (a), Kemmel1 sandy loam (b), Kemmel2 loam (c), and the combined data from three soils (d) with the models of $Q_s = k_1 KE^{a_1} u_*^{b_1}$ and $q_s = k_2 KE^{a_2} q^{b_2} S^{c_2}$.

error to the variance in the measured data:

$$E = 1 - \frac{\sum_{i=1}^{n} (Q_{s_{mi}} - Q_{s_{pi}})^2}{\sum_{i=1}^{n} (Q_{s_{pi}} - \bar{Q}_s)^2} \tag{20}$$

where $Q_{s_{mi}}$ and $Q_{s_{pi}}$ are the measured and predicted rainsplash data, respectively, and $\bar{Q}_s$ is the measured mean. High values of E indicated better agreement between the measured and predicted rainsplash transport (Table 3, Fig. 1).

The form of the model developed above features an integration of wind effects on the physical raindrop impact, and hence detachment, and on the transport process. Because previous mathematical models of rainsplash erosion developed for windless rain did not include the roles of wind in both detachment and transport processes (Savat and Poesen, 1981; Poesen, 1985, 1986; Wright, 1986, 1987), they are unlikely to be suitable for modeling the process under wind-driven rains. In this experimental study, wind increased the raindrop resultant velocity and altered the angle of raindrop incidence, which resulted in a variable raindrop impact frequency and impact angle. Therefore, differential delivery rates occurred depending on the variations in raindrop trajectory and frequency

with wind velocity and direction. More significantly, the wind had a greater effect on transport than slope gradient.

3.2. Sediment transport by rain-impacted thin flow

As soon as runoff started, the flow-driven process began to transport the detached soil particles. The rates of sediment transported by rain-impacted thin flow for three soils are presented in Table 4. Time to runoff varied depending on the actual amount of rain intercepted by the soil surface, which was a function of rain inclination and slope gradient and aspect. The effect of slope aspect on rain interception and runoff generation was stronger for the higher wind velocities: the angle of rain incidence attained very high values as rain inclination and the slope gradient increased in leeward slopes, resulting in very low intensity values. For example, the overland flow generation was retarded approximately for 45 min under the rains driven by the wind velocities of 10 and 14 m s^{-1} on the leeward slopes of 7, 15, and 20%. When the rain intensity was less than 60 mm h^{-1}, the wind-driven rainsplash process lasted longer than

Table 4

Summary of the data used in evaluating sediment transport by the rain-impacted thin flow (q_s) for three soils

u (m s^{-1})	S (m m^{-1})	Nukerke			Kemmel1			Kemmel2			n
		q (m^2 min^{-1})	q_s (g m^{-1}min^{-1})		q (m^2 min^{-1})	q_s (g m^{-1} min^{-1})		q (m^2 min^{-1})	q_s (g m^{-1} min^{-1})		
			Mean	Stdev.		Mean	Stdev.		Mean	Stdev.	
0-ww	0.07	3.878E − 04[a]	23.98	2.41	4.935E − 04	16.56	5.42	3.243E − 04	20.13	0.84	3
	0.15	4.888E − 04	29.95	3.59	5.100E − 04	38.39	5.94	3.540E − 04	22.76	0.96	3
	0.20	4.938E − 04	45.07	4.01	5.237E − 04	37.50	1.83	3.831E − 04	41.66	2.12	3
6-ww	0.07	4.308E − 04	11.35	0.50	2.715E − 04	5.35	0.12	2.348E − 04	8.00	0.82	3
	0.15	5.461E − 04	29.93	3.14	3.769E − 04	18.84	0.91	2.022E − 04	12.59	2.04	3
	0.20	5.756E − 04	45.39	3.49	4.755E − 04	33.17	2.01	2.400E − 04	22.34	4.78	3
10-ww	0.07	5.883E − 04	26.28	1.22	5.497E − 04	17.15	1.64	2.562E − 04	20.65	4.53	3
	0.15	7.367E − 04	66.90	11.09	6.464E − 04	61.92	8.48	3.429E − 04	38.51	10.91	3
	0.20	7.926E − 04	104.45	8.45	7.445E − 04	121.95	5.98	3.468E − 04	49.88	2.65	3
14-ww	0.07	4.788E − 04	21.40	1.68	4.087E − 04	14.98	3.84	2.380E − 04	11.49	0.49	3
	0.15	5.238E − 04	54.41	15.25	5.169E − 04	45.99	6.07	2.760E − 04	36.29	5.74	3
	0.20	6.046E − 04	81.08	22.17	5.867E − 04	92.19	6.37	3.288E − 04	55.75	3.43	3
0-lw	0.07	6.694E − 04	34.77	2.87	6.087E − 04	34.90	4.57	5.325E − 04	30.89	1.28	3
	0.15	6.673E − 04	39.60	2.44	4.929E − 04	49.48	2.12	4.642E − 04	30.47	3.89	3
	0.20	8.286E − 04	63.19	3.06	5.954E − 04	59.95	5.76	6.555E − 04	55.91	7.23	3
6-lw	0.07	5.516E − 04	14.38	0.90	2.963E − 04	9.81	0.51	4.073E − 04	14.43	0.56	3
	0.15	4.384E − 04	17.01	0.79	2.218E − 04	10.35	0.59	2.212E − 04	8.22	0.28	3
	0.20	3.955E − 04	19.70	0.97	1.801E − 04	8.25	0.51	1.448E − 04	5.59	0.41	3
10-lw	0.07	3.899E − 04	14.75	0.33	1.899E − 04	6.99	0.38	1.943E − 04	11.68	0.68	3
	0.15	1.644E − 04	8.30	1.29	1.003E − 04	3.23	0.21	8.110E − 05	4.52	0.65	3
	0.20	1.363E − 04	5.70	0.36	6.925E − 05	1.89	0.13	4.554E − 05	1.85	0.28	3
14-lw	0.07	1.756E − 04	9.94	0.71	1.117E − 04	5.76	0.30	9.650E − 05	8.16	0.58	3
	0.15	8.300E − 05	6.81	1.00	5.328E − 05	2.63	0.12	6.273E − 05	3.00	0.25	3
	0.20	6.707E − 05	4.98	0.19	4.137E − 05	1.03	0.05	4.314E − 05	1.80	0.20	3

Mean values are given in the table, however, statistical analyses are performed with individual data points. u, horizontal wind velocity (ww: windward; lw: leeward); S, channel bottom slope; q, unit discharge.

[a] The E notation means times 10 to the power.

the thin flow-driven process due to the retarded flow generation. Evidently, the wind effect was not only on the rainsplash detachment by changing velocity, frequency, and angle of the impinging raindrops but also on the flow generation, which demarcated the dominant transport process.

The statistical fit of Eq. (16), which is based on the interaction between raindrop impact and flow parameters (Julien and Simon, 1985; Gilley et al., 1985; Guy et al., 1987; Zhang et al., 1998), are shown in Table 5. The fluxes of rain energy and momentum adequately described the characteristics of wind-driven rains for the interrill sediment delivery to the thin flow transport as well as to the rainsplash transport. The analysis of variance showed that a_2 was significant at the level of $\alpha = 0.05$ for each case. Compared to the impact of raindrops on bare soil, lesser a_2 values for fluxes of rain energy and momentum suggested the detaching power of raindrops was partially dispersed by the thin flow depth on the soil surface (Moss and Green, 1983; Torri et al., 1987; Kinnell, 1991). The relative soil transport parameter for thin flow-driven process (k_2) and exponent values to which the unit discharge and slope were raised (b_2 and c_2, respectively) were also significant at the level of $\alpha = 0.05$ for all cases (Table 5). Equations developed using rain energy flux

for all data are:

$$q_s = 4.34E - 04KE^{0.37}q^{0.72}S^{0.53} \qquad (21)$$

$$q_s = 9.33E - 04KE^{0.53}q^{0.75}S^{0.57} \qquad (22)$$

The units of variables are as presented in Tables 1 and 4. In general, the models performed reasonably well, accounted for $\geq 89\%$ of the variations in the shallow flow transport rates, and indicated $\geq 74\%$ of efficiencies (Fig. 1).

3.3. Total sediment transport from interrill areas

Values of total sediment transport (Eq. (17)) are presented in Table 6 along with the ratio of rainsplash erosion to the corresponding total sediment transport ($R = Q_s/q_i$). Results showed that, for all cases of windless rains, R varied from 2 to 6%, with a mean of 2.8%. This finding was consistent with the previous research by Moss and Green (1983), Walker et al. (1978), and Moss (1988), and confirmed the fact that the contribution of the rainsplash transport is very small and negligible compared to that of sediment transport by shallow overland flow (Kinnell, 1991; Hairsine and Rose, 1991; Parsons et al., 1994; Sharma et al., 1995).

For all soils, however, the results with wind indicated that mean R-values ranged from 8 to 27%,

Table 5
Statistical analyses for the equation of sediment transport by the rain-impacted thin flow (q_s) developed by log-linear regression technique for three soils and the combined data from three soils

Soil	$q_s = k_2KE^{a_2}q^{b_2}S^{c_2}$									
	k_2	Prob > |T|	a_2	Prob > |T|	b_2	Prob > |T|	c_2	Prob > |T|	R^2	E^a
Nukerke	3.33E − 03	0.0001	0.45	0.0001	0.34	0.0034	0.65	0.0001	0.91	0.77
Kemmel1	4.74E − 04	0.0001	0.51	0.0002	0.67	0.0009	0.73	0.0001	0.94	0.78
Kemmel2	2.27E − 03	0.0001	0.55	0.0001	0.39	0.0079	0.31	0.0004	0.91	0.81
All data	4.34E − 04	0.0001	0.37	0.0001	0.72	0.0001	0.53	0.0001	0.90	0.79
	$q_s = k_2M^{a_2}q^{b_2}S^{c_2}$									
	k_2	Prob > |T|	a_2	Prob > |T|	b_2	Prob > |T|	c_2	Prob > |T|	R^2	E
Nukerke	5.75E − 03	0.0001	0.71	0.0001	0.31	0.0208	0.65	0.0001	0.90	0.74
Kemmel1	2.48E − 05	0.0001	0.63	0.0029	0.82	0.0001	0.72	0.0001	0.94	0.77
Kemmel2	4.64E − 03	0.0001	0.85	0.0001	0.36	0.0365	0.30	0.0012	0.90	0.78
All data	9.33E − 04	0.0001	0.53	0.0001	0.75	0.0001	0.57	0.0001	0.89	0.77

[a] The coefficient of efficiency (Eq. (20)).

Table 6
Summary of the data for the total interrill erosion measured by the rainsplash and flow-driven transport for three soils

u (m s^{-1})	S (m m^{-1})	Nukerke				Kemmel1				Kemmel2			
		Q_s (g m^{-1} min^{-1})	q_s (g m^{-1} min^{-1})	q_i (g m^{-1} min^{-1})	R (g m^{-1} min^{-1})	Q_s (g m^{-1} min^{-1})	q_s (g m^{-1} min^{-1})	q_i (g m^{-1} min^{-1})	R (g m^{-1} min^{-1})	Q_s (g m^{-1} min^{-1})	q_s (g m^{-1} min^{-1})	q_i (g m^{-1} min^{-1})	R (g m^{-1} min^{-1})
0-ww	0.07	0.64	23.98	24.63	0.03	1.02	16.56	17.58	0.06	0.49	20.13	20.62	0.02
	0.15	0.90	29.95	30.85	0.03	1.31	38.39	39.70	0.03	1.47	22.76	24.23	0.06
	0.20	1.59	45.07	46.65	0.03	1.47	37.50	38.97	0.04	1.25	41.66	42.92	0.03
6-ww	0.07	2.25	11.35	13.61	0.17	2.02	5.35	7.37	0.27	1.69	8.00	9.69	0.17
	0.15	2.81	29.93	32.74	0.09	3.11	18.84	21.95	0.14	2.24	12.59	14.83	0.15
	0.20	4.21	45.39	49.60	0.08	3.80	33.17	36.97	0.10	2.74	22.34	25.08	0.11
10-ww	0.07	11.03	26.28	37.32	0.30	9.02	17.15	26.18	0.34	8.91	20.65	29.56	0.30
	0.15	11.03	66.90	77.93	0.14	10.70	61.92	72.62	0.15	10.73	38.51	49.25	0.22
	0.20	16.03	104.45	120.47	0.13	20.83	121.95	142.79	0.15	12.90	49.88	62.79	0.21
14-ww	0.07	16.65	21.40	38.05	0.44	11.70	14.98	26.68	0.44	10.81	11.49	22.30	0.48
	0.15	29.41	54.41	83.82	0.35	23.64	45.99	69.64	0.34	25.76	36.29	62.05	0.42
	0.20	41.60	81.08	122.68	0.34	35.91	92.19	128.10	0.28	38.78	55.75	94.53	0.41
0-lw	0.07	0.60	34.77	35.37	0.02	0.54	34.90	35.44	0.02	0.71	30.89	31.60	0.02
	0.15	0.75	39.60	40.35	0.02	0.91	49.48	50.40	0.02	1.09	30.47	31.57	0.03
	0.20	1.19	63.19	64.38	0.02	1.31	59.95	61.26	0.02	1.18	55.91	57.10	0.02
6-lw	0.07	4.49	14.38	18.88	0.24	1.27	9.81	11.08	0.11	2.73	14.43	17.16	0.16
	0.15	1.54	17.01	18.55	0.08	0.86	10.35	11.22	0.08	2.78	8.22	10.99	0.25
	0.20	1.62	19.70	21.32	0.08	1.12	8.25	9.37	0.12	1.57	5.59	7.16	0.22
10-lw	0.07	4.31	14.75	19.06	0.23	3.72	6.99	10.71	0.35	3.21	11.68	14.90	0.22
	0.15	1.50	8.30	9.80	0.15	1.09	3.23	4.32	0.25	1.58	4.52	6.10	0.26
	0.20	1.58	5.70	7.28	0.22	0.96	1.89	2.85	0.34	1.07	1.85	2.92	0.37
14-lw	0.07	5.16	9.94	15.09	0.34	7.32	5.76	13.08	0.56	5.68	8.16	13.84	0.41
	0.15	2.74	6.81	9.56	0.29	1.56	2.63	4.19	0.37	2.00	3.00	5.00	0.40
	0.20	1.10	4.98	6.08	0.18	0.95	1.03	1.98	0.48	0.92	1.80	2.72	0.34

u, horizontal wind velocity (ww: windward; lw: leeward); S, channel bottom slope; Q_s, transport rate by the rainsplash; q_s, transport rate by the rain-impacted shallow overland flow; q_i, total sediment transport rate ($q_i = Q_s + q_s$); R, the ratio of the rainsplash transport rate to the total sediment transport rate ($R = Q_s/q_i$).
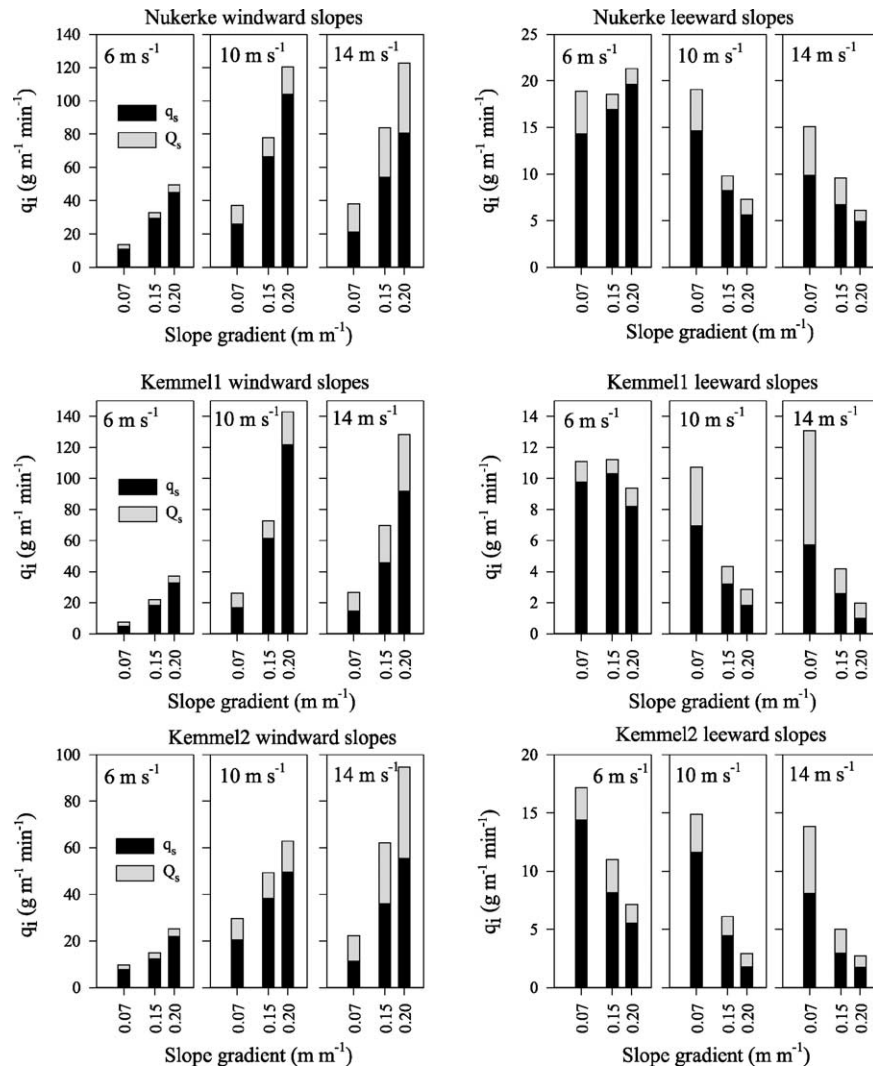
Fig. 2. Total sediment transport from interrill areas based on the wind-driven rainsplash and the sediment transport by the rain-impacted thin flow for three soils.

from 13 to 37%, and from 18 to 56%, and the mean values were 14.6 ± 6.4, 23.9 ± 7.8, and $38.1 \pm 8.7\%$ for the rains driven by 6, 10, and 14 m s^{-1} wind, respectively. The stacked bar graphs of total sediment transport with the components of the wind-driven rainsplash and flow-driven transport are illustrated in Fig. 2. Evidently, in our study the rainsplash transport was a significant process to the extent that it should not be neglected in accurately predicting water erosion soil losses from interrill areas.

4. Conclusions

In this study with wind-driven rains, sediment transport from interrill areas was achieved by two distinct mechanisms, rainsplash and thin flow transport, mainly differentiated in terms of flow onset. The fluxes of rain energy and momentum computed by combining the effects of wind on the velocity, frequency, and angle of raindrop impact reasonably explained the characteristics of

wind-driven rains and significantly accounted for the differences in sediment delivery rates to either to the rainsplash or thin flow transport. Rainsplash transport for the three soils studied was adequately described by relating transport rate to the rain impact parameter, fluxes of rain energy and momentum, and the wind shear velocity. Equations developed incorporated the dynamic effects of physical raindrop impact and wind action on the process, therefore, provided a basis for modeling interrill rainsplash transport under wind-driven rains. So far, no known attempts except the present research have been made to combine the effects of rain and wind for modeling purposes. Unfortunately, our model is based on limited laboratory data, and thus research is needed for field-testing and verification.

Sediment transport by rain-impacted shallow flow was also adequately predicted by relating the transport rate to the rain impact parameter and the discharge and slope. Equations are based on the mechanics of interrill erosion and reflect the combined effect of raindrop impact and flow on the process.

Consequently, comparing the contributions of either process to the total sediment transport, we concluded that the wind-driven rainsplash transport was a significant process that should be considered to assess interrill erosion. The results can be used to improve the understanding of erosion processes and provide a better estimate of soil detachment and transport under wind-driven rainfall.

References

De Lima, J.L.M.P., 1989. Raindrop splash anisotropy: slope, wind, and overland flow velocity effects. Soil Technology 2, 71–78.

De Lima, J.L.M.P., 1990. The effect of oblique rain on inclined surfaces: a nomograph for the rain-gauge correction factor. Journal of Hydrology 115, 407–412.

De Lima, J.L.M.P., Van Dijk, P.M., Spaan, W.P., 1992. Splash-saltation transport under wind-driven rain. Soil Technology 5, 151–166.

Erpul, G., Gabriels, D., Janssens, D., 1998. Assessing the drop size distribution of simulated rainfall in a wind tunnel. Soil and Tillage Research 45, 455–463.

Erpul, G., Gabriels, D., Janssens, D., 2000. The effect of wind on size and energy of small simulated raindrops: a wind tunnel study. International Agrophysics 14, 1–7.

Gabriels, D., Cornelis, W., Pollet, I., Van Coillie, T., Quessar, M., 1997. The ICE wind tunnel for wind and water erosion studies. Soil Technology 10, 1–8.

Gilley, J.E., Finkner, S.C., 1985. Estimating soil detachment caused by raindrop impact. Transactions of the ASAE 28, 140–146.

Gilley, J.E., Woolhiser, D.A., McWhorter, D.B., 1985. Interrill soil erosion. Part I: development of model equations. Transactions of the ASAE 28, 147–153.see also p. 159.

Goossens, D., Poesen, J., Gross, J., Spaan, W., 2000. Splash drift on light sandy soils: a field experiment. Agronomie 20, 271–282.

Guy, B.T., Dickinson, W.T., Rudra, R.P., 1987. The roles of rainfall and runoff in the sediment transport capacity of interrill flow. Transactions of the ASAE 30, 1378–1386.

Hairsine, P.B., Rose, C.W., 1991. Rainfall detachment and deposition: sediment transport in the absence of flow driven processes. Soil Science Society of America Journal 55, 320–324.

Heymann, F.J., 1967. A survey of clues to the relation between erosion rate and impact parameters. Second Rain Erosion Conference 2, 683–760.

Julien, P.Y., Simon, D.B., 1985. Sediment transport capacity of overland flow. Transactions of the ASAE 28, 755–762.

Jungerius, P.D., Dekker, L.W., 1990. Water erosion in the dunes. Catena Supplement 18, 185–193.

Jungerius, P.D., Verheggen, A.J.T., Wiggers, A.J., 1981. The development of blowouts in De Blink, a coastal dune area near Noordwijkerout, the Netherlands. Earth Surface Processes and Landforms 6, 375–396.

Kinnell, P.I.A., 1991. The effect of flow depth on sediment transport induced by raindrops impacting shallow flows. Transactions of the ASAE 34, 161–168.

Kinnell, P.I.A., 1993. Interrill erodibilities based on the rainfall intensity-flow discharge erosivity factor. Australian Journal of Soil Research 31, 319–332.

Laws, J.O., 1941. Measurements of the fall velocity of water drops and raindrops. Transactions of the American Geophysical Union 22, 709–721.

Moeyersons, J., 1983. Measurements of splash-saltation fluxes under oblique rain. Catena Supplement 4, 19–31.

Moss, A.J., 1988. The effects of flow-velocity variations on rain-driven transportation and the role of rain impact in the movement of solids. Australian Journal of Soil Research 26, 443–450.

Moss, A.J., Green, P., 1983. Movement of solids in air and water by raindrop impact. Effects of drop-size and water-depth variations. Australian Journal of Soil Research 21, 373–382.

Nash, J.E., Sutcliffe, J.V., 1970. River flow forecasting through conceptual models. Part I: a discussion of principles. Journal of Hydrology 10, 282–290.

Nearing, M.A., Foster, G.R., Lane, L.J., Finkner, S.C., 1989. A Process based soil erosion model for USDA Water Erosion Prediction Project technology. Transactions of the ASAE 32, 1587–1593.

Parsons, A.J., Abrahams, A.D., Wainwright, J., 1994. Rainsplash and erosion rates in an interrill area on semi-arid grassland, Southern Arizona. Catena 22, 215–226.

Parsons, A.J., Stromberg, S.G.L., Greener, M., 1998. Sediment-transport competence of rain-impacted interrill overland flow. Earth Surface Processes and Landforms 23, 365–375.

Pedersen, H.S., Hasholt, B., 1995. Influence of wind speed on rainsplash erosion. Catena 24, 39–54.

Poesen, J., 1985. An improved splash transport model. Zeitschrift für Geomorphologie Neue Folge 29, 193–221.

Poesen, J., 1986. Field measurements of splash erosion to validate a splash transport model. Zeitschrift für Geomorphologie Neue Folge Supplementband 58, 81–91.

Poesen, J., Savat, J., 1981. Detachment and transportation of loose sediments by raindrop splash. Part II: detachability and transportability measurements. Catena 8, 19–41.

Rutin, J., 1983. Erosional processes on a coastal sand dune, De Blink, Noordwijkerhout. Laboratory of Physical Geography and Soil Science, University of Amsterdam, The Netherlands.

SAS, 1995. SAS System for Elementary Statistical Analysis, SAS Institute, Inc, Cary, NC, pp. 280–285.

Savat, J., Poesen, J., 1981. Detachment and transportation of loose sediments by raindrop splash. Part I: the calculation of absolute data on detachability and transportability. Catena 8, 1–18.

Sellers, W.D., 1965. Physical Climatology, University of Chicago Press, Chicago, IL, pp. 33–35.

Sensit™, 2000. Model V04, Kinetic Energy of Rain Sensor. Sensit Company, Portland, ND 58274-9607.

Sharma, P.P., Gupta, S.C., Foster, G.R., 1995. Raindrop-induced soil detachment and sediment transport from interrill areas. Soil Science Society of America Journal 59, 727–734.

Sharon, D., 1980. The distribution of hydrologically effective rainfall incident on sloping ground. Journal of Hydrology 46, 165–188.

Springer, G.S., 1976. Erosion by Liquid Impact, Wiley, New York.

Torri, D., Sfalanga, M., Del Sette, M., 1987. Splash detachment: runoff depth and soil cohesion. Catena 14, 149–155.

Umback, C.R., Lembke, W.D., 1966. Effects of wind on falling water drops. Transactions of the ASAE 9, 805–808.

Van Dijk, P.M., Stroosnijder, L., De Lima, J.L.M.P., 1996. The influence of rainfall on transport of beach sand by wind. Earth Surface Processes and Landforms 21, 341–352.

Van Heerden, W.M., 1967. An analysis of soil transportation by raindrop splash. Transactions of the ASAE 10, 166–169.

Walker, P.H., Kinnell, P.I.A., Green, P., 1978. Transport of noncohesive sandy mixture in rainfall and runoff experiments. Soil Science Society of America Journal 42, 793–801.

Wright, A.C., 1986. A physically-based model of the dispersion of splash droplets ejected from a water drop impact. Earth Surface Processes and Landforms 11, 351–367.

Wright, A.C., 1987. A model of the redistribution of disaggregated soil particles by rainsplash. Earth Surface Processes and Landforms 12, 583–596.

Zhang, X.C., Nearing, M.A., Miller, W.P., Norton, L.D., West, L.T., 1998. Modeling interrill sediment delivery. Soil Science Society of America Journal 62, 438–444.